Supplementary Materials for

Therapeutic decoupling of restenosis prevention from impaired vascular healing with regenerative nanovesicle-eluting bioresorbable scaffolds

Min-Kyu Kang[1,†], Ji Won Kim[2,3,†], Yu-Jeong Lee[1,†], Dong-Sung Won[2,3], Gi Wook Lee[4], Weiqiang Liu[5], Chae-lin Kim[6], Su-Hyun Park[1], Ju-El Kim[1], Tae-Hyun Heo[1], Seung Jin Eo[2,3], Gun-Jae Jeong[7], Ilkoo Noh[8,9], Min-Ho Kang[10], Han Young Kim[10], Young Min Shin[11], Jung Bok Lee[12], Minseo Park[6], Hyun-Ji Park[6], Rosaire Mongrain[5], Hyung Il Kim[4], Jung-Hoon Park[2,3,*], Jeong-Kee Yoon[1,*]

[1] Department of Systems Biotechnology, Chung-Ang University, Anseong-Si, Gyeonggi-Do 17546, Republic of Korea

[2] Biomedical Engineering Research Center, Asan Institute for Life Sciences, Asan Medical Center, Seoul 05505, Republic of Korea

[3] Department of Convergence Medicine, Asan Medical Center, University of Ulsan College of Medicine, Seoul 05505, Republic of Korea

[4] Dotter Co. Ltd., Incheon 22007, Republic of Korea

[5] Department of Mechanical Engineering, McGill University, Montréal, QC, H3A 0C3, Canada

[6] Department of Molecular Science and Technology, Ajou University, Suwon 16499, Republic of Korea

[7] School of Nanomedical Engineering, Korea National University of Transportation, Chungju-si, Chungbuk 27469, Republic of Korea

[8] Department of Biomedical Technology, Kangwon National University, Chuncheon 24341, Republic of Korea

[9] Institute of Bioscience & Biotechnology, Kangwon National University, Chuncheon 24341, Republic of Korea

[10] Department of Biomedical-Chemical Engineering, The Catholic University of Korea, Bucheon-si, Gyeonggi-do, Republic of Korea

[11] Institute of Cell and Tissue Engineering, College of Medicine, The Catholic University of Korea, Seoul 06591, Republic of Korea

[12] Department of Biological Science, Research Institute of Women's Health, Brain Korea 21 Project, Sookmyung Women's University, Seoul 04310, Republic of Korea

[†] These authors contributed equally to this work as co-first authors.

[*] Corresponding Authors:

Jeong-Kee Yoon, Ph.D. (E-mail: jyoon342@cau.ac.kr)

Jung-Hoon Park, Ph.D. (E-mail: jhparkz@amc.seoul.kr)

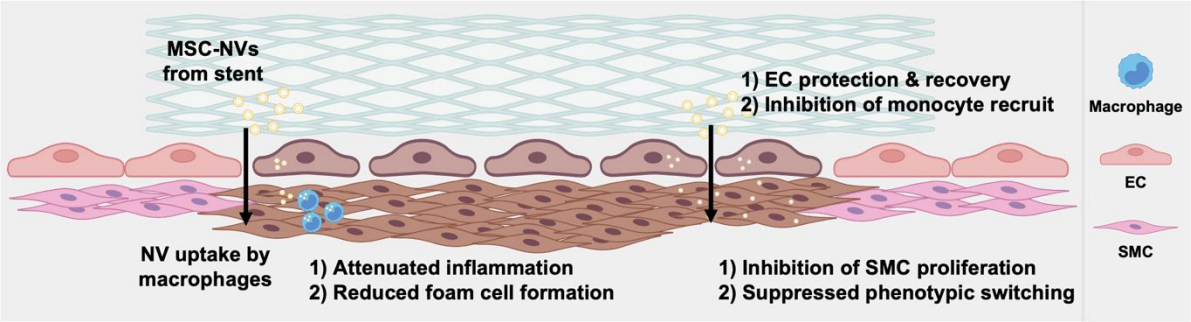


Figure S1. Schematic illustration of stent-mediated local delivery of MSC-NVs for vasculomodulation. MSC-NVs are internalized by macrophages, ECs, and SMCs, leading to attenuation of inflammatory activation, promotion of endothelial repair, and suppression of SMC proliferation and phenotypic modulation.

Table S1. Angiographic, optical coherence tomographic (OCT), and histologic findings in the rabbit iliac artery.

	Bare BRS group	NVE-BRS group	p-value*
Angiography			
§Luminal diameter change (%)	23.32 ± 9.45	8.50 ± 3.48	0.005*
OCT			
Luminal diameter (mm)	1.92 ± 0.02	2.23 ± 0.23	< 0.001*
Neointimal thickness (mm)	0.40 ± 0.02	0.17 ± 0.01	< 0.001*
Stenosis area (%)	48.80 ± 1.56	19.38 ± 1.67	< 0.001*
Histology			
Inflammatory cell infiltration (Degree)	3.30 ± 0.15	1.2 ± 0.13	< 0.001&
Fibrin deposition (Degree)	3.10 ± 0.37	1.40 ± 0.16	< 0.001&
Collagen deposition (Degree)	3.60 ± 0.16	1.3 ± 0.15	< 0.001&
Elastic lamina change (Degree)	2.3 ± 0.31	1.1 ± 0.08	< 0.001&
Immunofluorescence			
PDGFR-β-positive deposition (Degree)	4.4 ± 0.16	1.5 ± 0.16	< 0.001&
α-SMA-positive deposition (Degree)	4.7 ± 0.15	1.9 ± 0.17	< 0.001&
VCAM-1-positive deposition (Degree)	3.8 ± 0.13	1.1 ± 0.10	< 0.001&

CD68-positive deposition (Degree)	4.4 ± 0.16	2.0 ± 0.14	< 0.001[&]
CD31-positive deposition (Degree)	1.3 ± 0.15	2.6 ± 0.16	< 0.001[&]

Note. Data are presented as mean ± standard deviation (SD). [§]The amount of change was calculated as the difference between post-procedural measurements and those obtained at the one-month follow-up. The remaining variables were obtained at follow-up. *Statistical analysis was performed using the *two-sample t-test or the [&]Mann–Whitney U test.

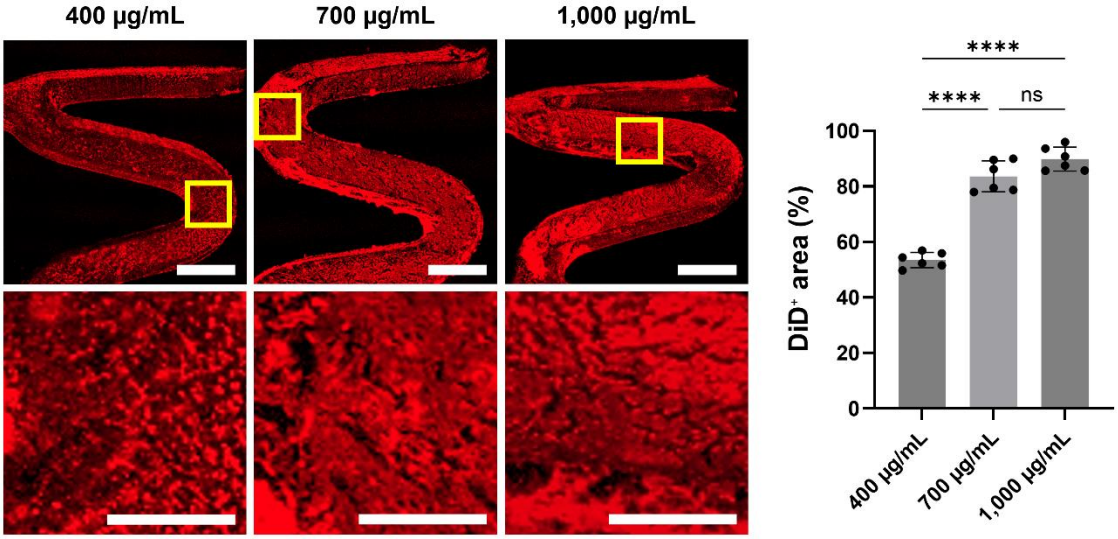


Figure S2. Effect of MSC-NV concentration on NVE-BRS coating efficiency. Representative confocal fluorescence images of NVE-BRSs coated with DiD-labeled MSC-NVs at concentrations of 400, 700, and 1,000 μg/mL in PBS. The lower panels show magnified views of the regions indicated by the yellow boxes. DiD-positive coating area was quantified as a percentage of the scaffold area (n = 6). Scale bars = 250 μm in the upper panels and 100 μm in the lower panels. Quantitative data are expressed as the mean ± SD. Comparisons among groups were performed using one-way ANOVA followed by Tukey's multiple-comparisons test. ns = non-significant; ****$p < 0.0001$.

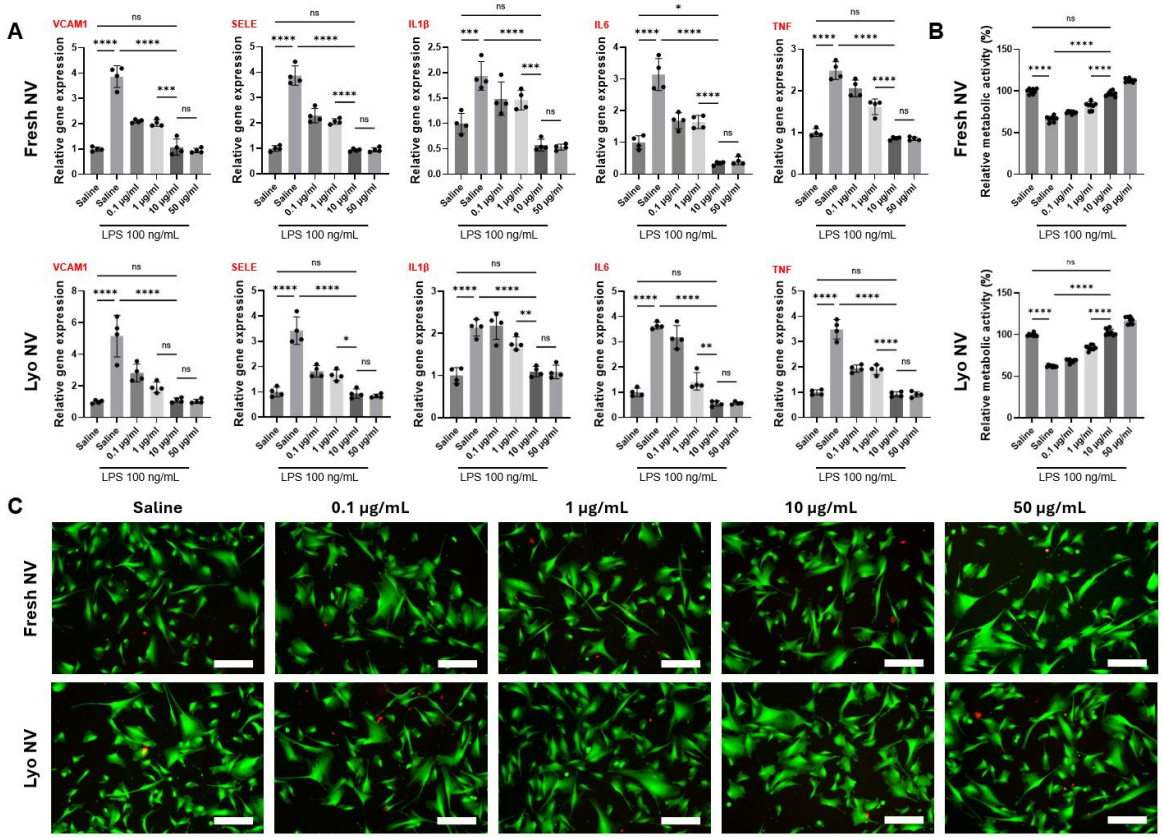


Figure S3. Dose-dependent effects of MSC-NVs on inflammatory responses and cellular activity in hCAECs. (A) Relative mRNA expression of *VCAM1*, *SELE*, *IL1B*, *IL6*, and *TNF* in human coronary artery endothelial cells (hCAECs) treated with Fresh- or Lyo-NVs at 0.1, 1, 10, or 50 μg/mL under LPS stimulation (100 ng/mL, 6 h), as determined via qRT-PCR (n = 4). (B) Relative metabolic activity of LPS-stimulated hCAECs following treatment with Fresh- or Lyo-NVs at the indicated concentrations, as determined by CCK-8 assay (n = 8). For (A) and (B), the first Saline group represents the non-stimulated vehicle control, whereas the second Saline group represents the LPS-stimulated vehicle control. The horizontal bar labeled "LPS 100 ng/mL" indicates all LPS-stimulated groups, including the second Saline group and the MSC-NV-treated groups. (C) Representative Live/Dead fluorescence images of hCAECs treated with Fresh- or Lyo-NVs alone at the indicated concentrations for 6 h without LPS stimulation. Live and dead cells are shown in green and red, respectively. Scale bar = 200 μm. Quantitative data are expressed as the mean ± SD. Comparisons among groups were performed using one-way ANOVA followed by Tukey's multiple comparisons test. ns = non-significant, *$p < 0.05$, **$p < 0.01$, ***$p < 0.001$, ****$p < 0.0001$.

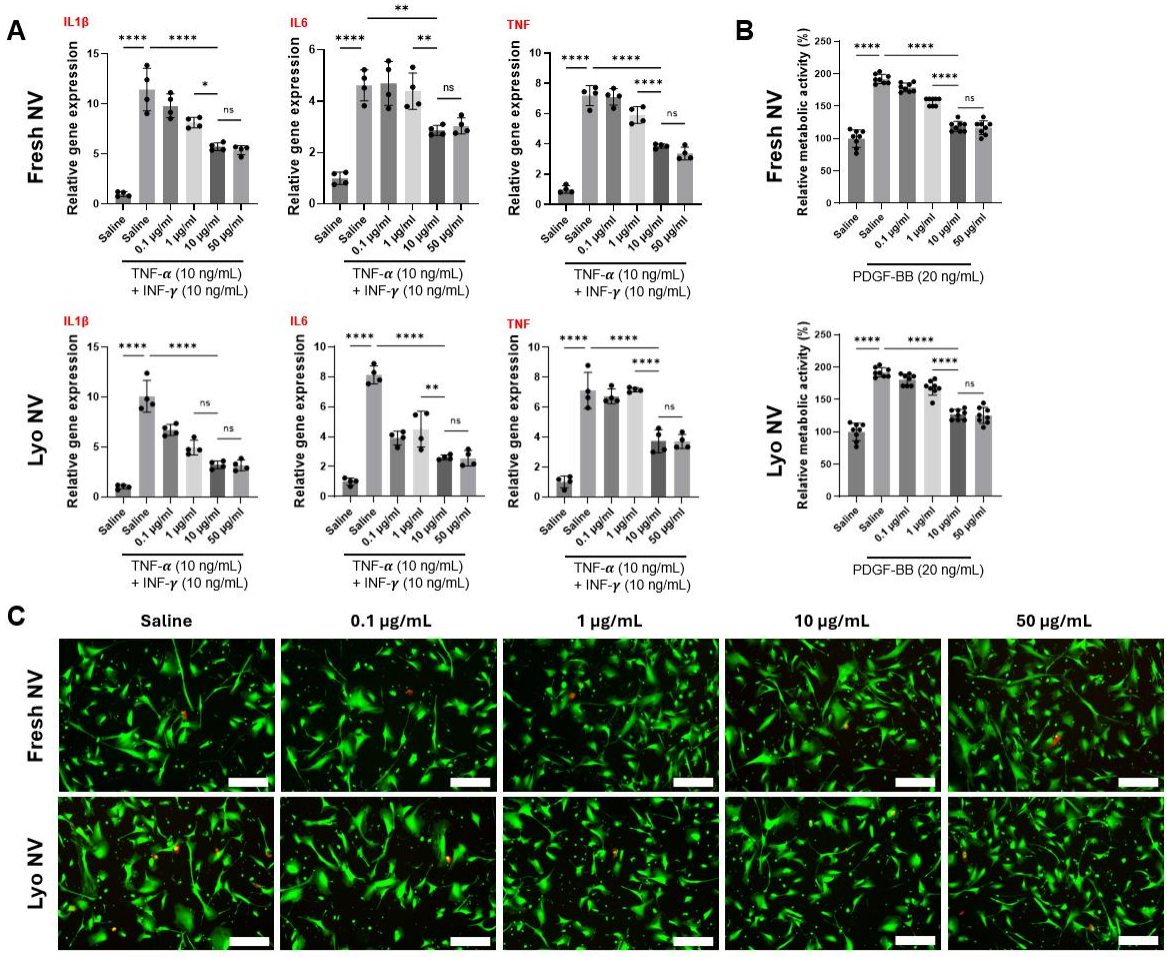


Figure S4. Dose-dependent effects of MSC-NVs on inflammatory and proliferative responses in hAoSMCs. (A) Relative mRNA expression of *IL1B*, *IL6*, and *TNF* in human aortic smooth muscle cells (hAoSMCs) treated with Fresh- or Lyo-NVs at 0.1, 1, 10, or 50 μg/mL under TNF-α and IFN-γ stimulation (10 ng/mL each, 6 h), as determined via qRT-PCR (n = 4). The first Saline group represents the non-stimulated vehicle control, whereas the second Saline group represents the cytokine-stimulated vehicle control. The horizontal bar labeled "TNF-α (10 ng/mL) + IFN-γ (10 ng/mL)" indicates all cytokine-stimulated groups, including the second Saline group and the MSC-NV-treated groups. (B) Relative metabolic activity of PDGF-BB-stimulated hAoSMCs (20 ng/mL, 48 h) following treatment with Fresh- or Lyo-NVs at the indicated concentrations, as determined using the CCK-8 assay (n = 8). The first Saline group represents the non-stimulated vehicle control, whereas the second Saline group represents the PDGF-BB-stimulated vehicle control. The horizontal bar labeled "PDGF-BB (20 ng/mL)" indicates all PDGF-BB-stimulated groups, including the second Saline group and the MSC-NV-treated groups. qRT-PCR and CCK-8 results were normalized to the corresponding non-stimulated vehicle control. (C) Representative Live/Dead fluorescence images of hAoSMCs

treated with Fresh- or Lyo-NVs alone at the indicated concentrations for 6 h without inflammatory or proliferative stimulation. Live and dead cells are shown in green and red, respectively. Scale bar = 200 μm. Quantitative data are expressed as the mean ± SD. Comparisons among groups were performed using one-way ANOVA followed by Tukey's multiple comparisons test. ns = non-significant, *$p < 0.05$, **$p < 0.01$, ***$p < 0.001$, ****$p <$ 0.0001.

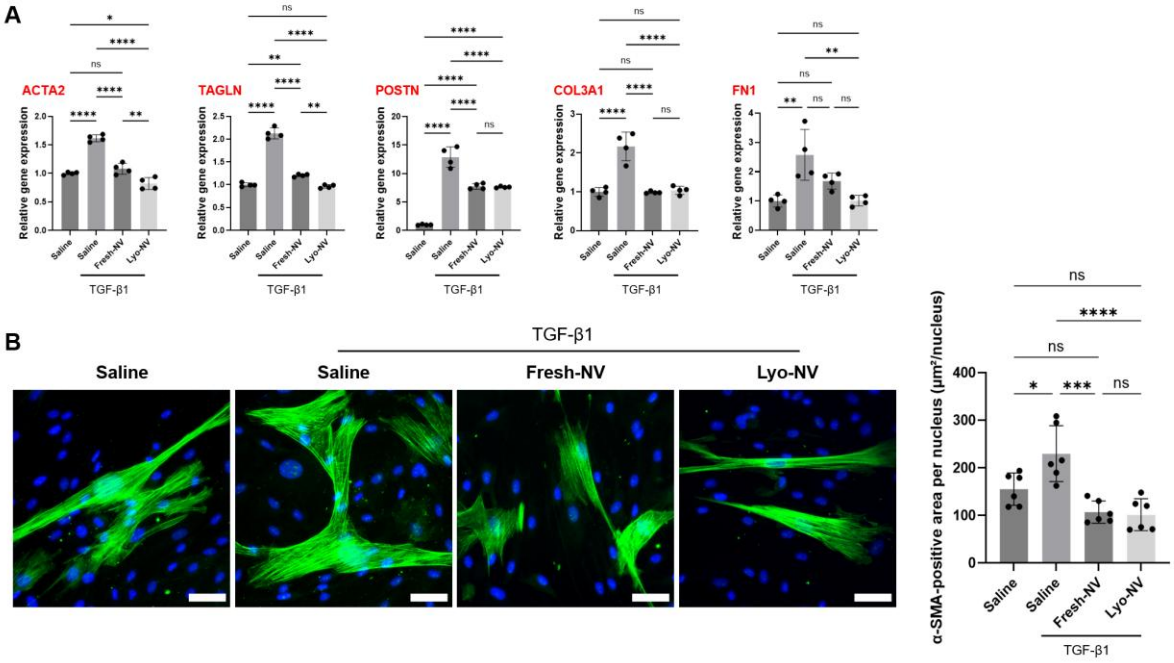


Figure S5. MSC-NVs attenuate TGF-β1-induced activation of human vascular adventitial fibroblasts. (A) Relative mRNA expression of *ACTA2*, *TAGLN*, *POSTN*, *COL3A1*, and *FN1* in human vascular adventitial fibroblasts (hBVAFs) stimulated with TGF-β1 (10 ng/mL) and treated with Fresh- or Lyo-NVs at 10 μg/mL for 48 h, as determined via qRT-PCR (n = 4). Expression levels were normalized to the non-stimulated vehicle control. (B) Representative immunofluorescence images of α-SMA (green) and DAPI-stained nuclei (blue), with quantification of the α-SMA-positive area per nucleus (n = 6). In both panels, the first Saline group represents the non-stimulated vehicle control. The horizontal bar labeled "TGF-β1" identifies the second Saline, Fresh-NV, and Lyo-NV groups as TGF-β1-stimulated; accordingly, the second Saline group represents the TGF-β1-stimulated vehicle control. Scale bar = 50 μm. Quantitative data are expressed as the mean ± SD. Comparisons among groups were performed using one-way ANOVA followed by Tukey's multiple comparisons test. ns = non-significant, *$p < 0.05$, **$p < 0.01$, ***$p < 0.001$, ****$p < 0.0001$.

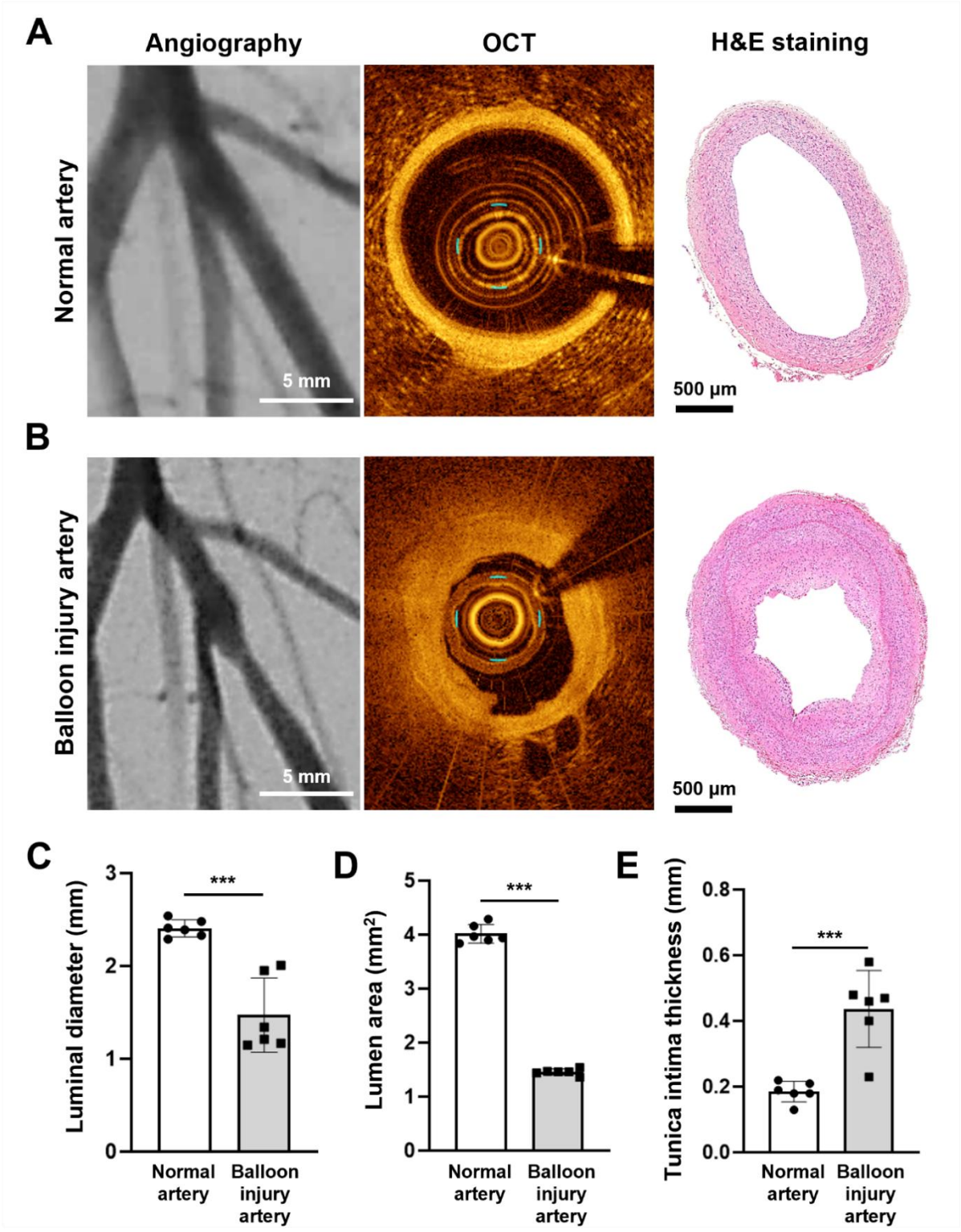


Figure S6. Establishment and validation of the balloon injury artery model before bioresorbable scaffold (BRS) implantation. Representative angiographic, optical coherence tomography (OCT), and hematoxylin and eosin (H&E) staining images of (A) normal iliac arteries and (B) balloon-injured iliac arteries at 1 week after balloon injury. Balloon-injured

arteries exhibited marked luminal narrowing and neointimal thickening compared with normal arteries. (C) Quantitative angiographic analysis of luminal diameter. (D) Quantitative OCT analysis of lumen area. (E) Quantification of tunica intima thickness based on H&E-stained sections. Data are presented as mean ± SD. Statistical comparisons were performed using a two-sample t-test. ***$p < 0.001$. Scale bars: angiography, 5 mm; H&E staining, 500 μm.

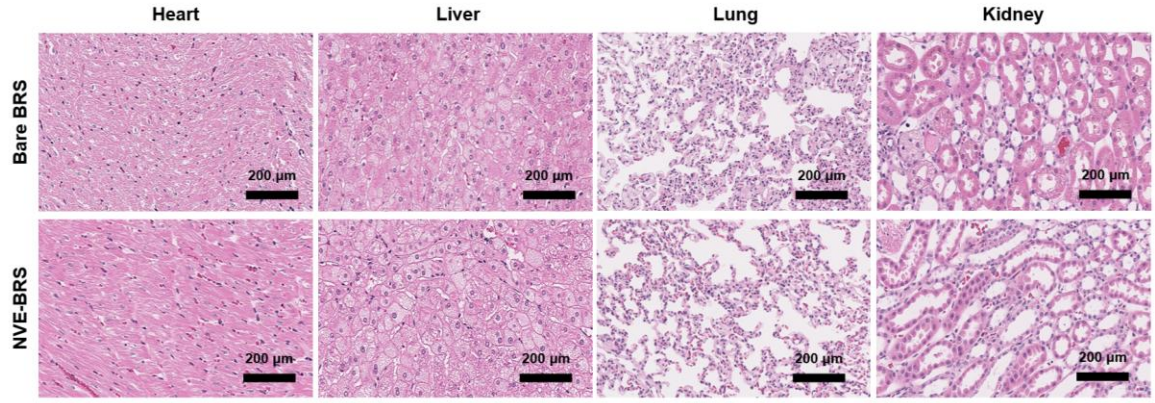


Figure S7. Histopathological evaluation of major organs following NVE-BRS implantation. No significant difference was observed from representative H&E-stained sections of the heart, liver, lung and kidney harvested 4 weeks after implantation from the bare BRS and NVE-BRS groups.

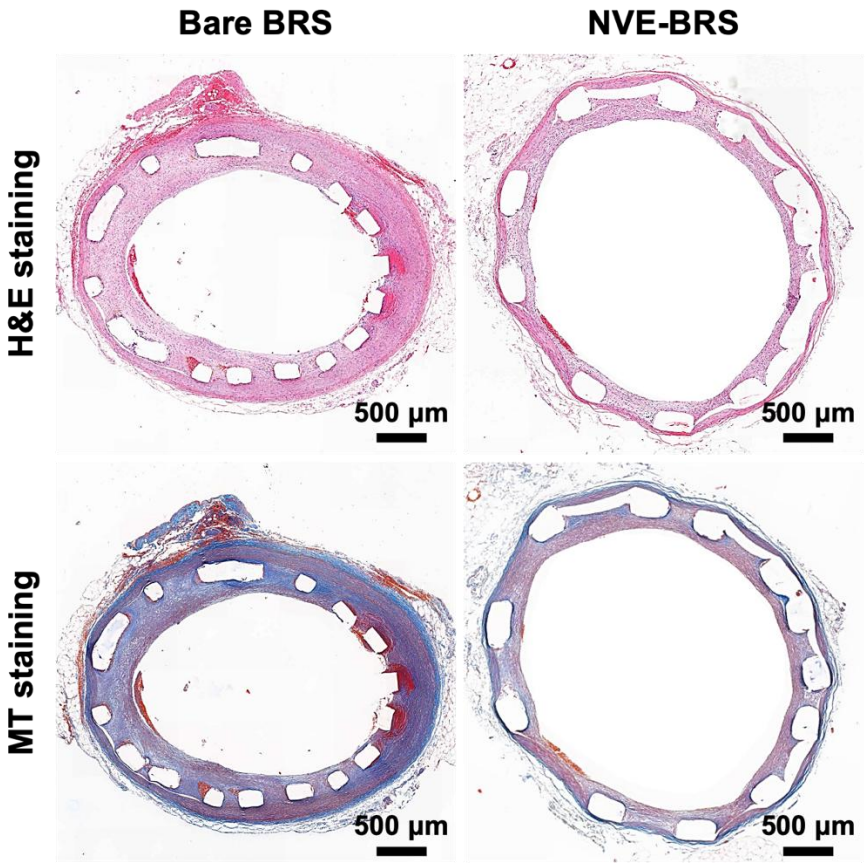


Figure S8. Representative microscopic images of H&E and Masson's trichrome (MT) stained histological sections obtained 4 weeks after BRS placement in a balloon injured rabbit iliac artery model.

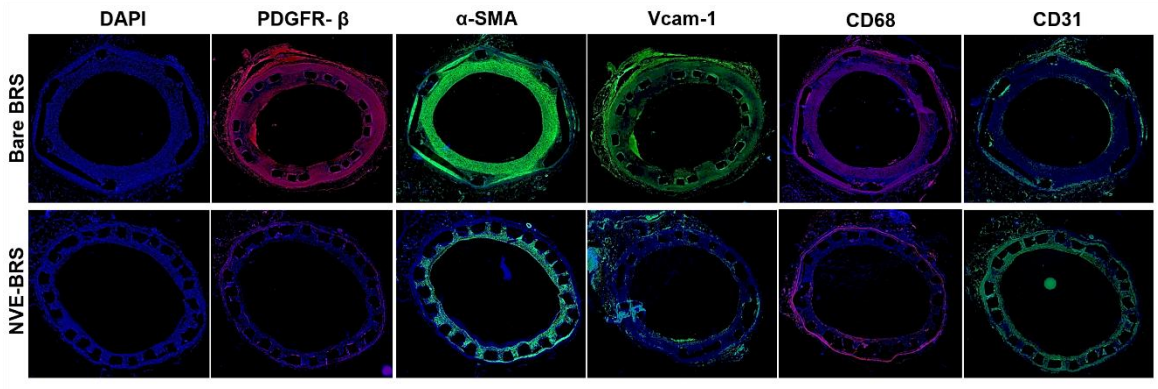


Figure S9. Representative immunofluorescence images obtained at 4 weeks after BRS placement in the study groups. Representative low-magnification fluorescence images of entire vessel cross-sections stained for platelet-derived growth factor receptor-β (PDGFR-β), α-smooth muscle actin (α-SMA), vascular cell adhesion molecule-1 (VCAM-1), CD68, and CD31 are shown for the study groups. Representative images demonstrate differences in

vascular remodeling and inflammatory responses between the two groups.

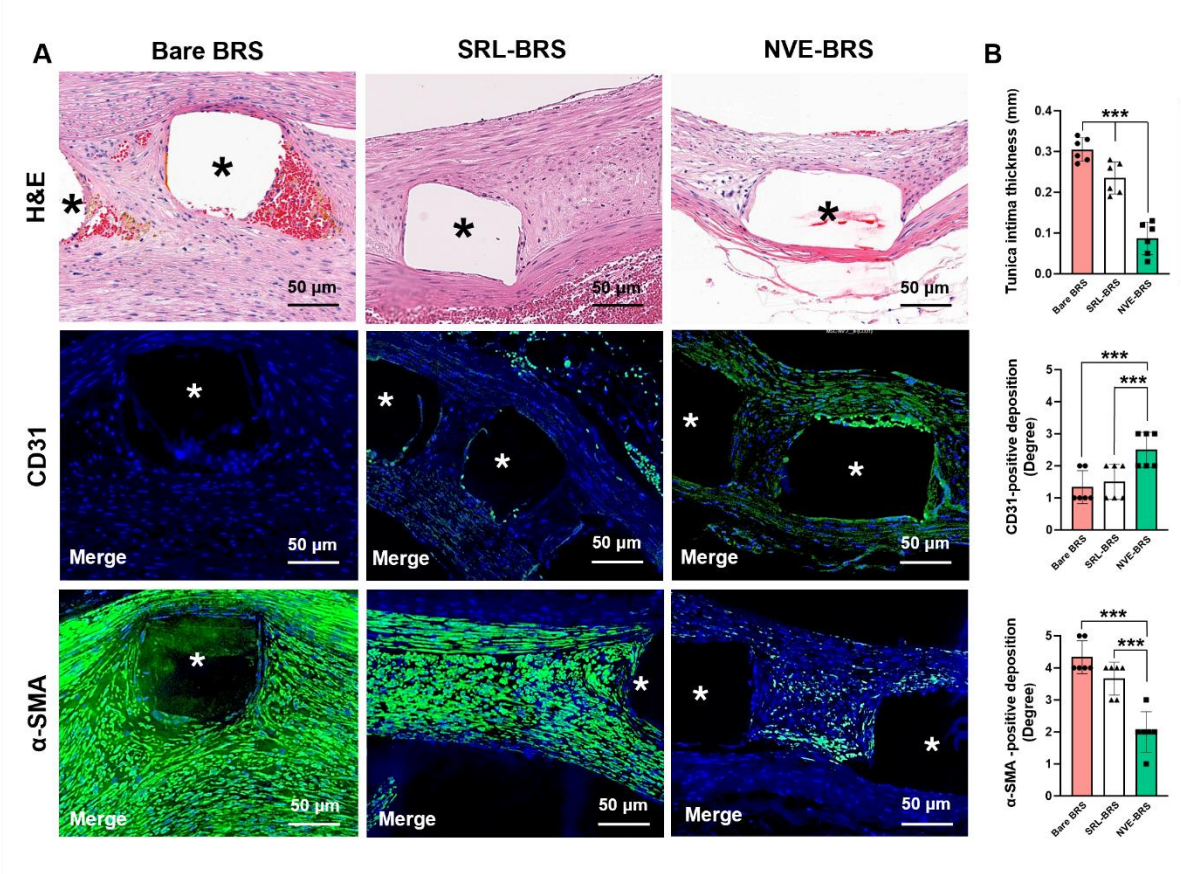


Figure S10. Histological and immunofluorescence evaluation of vascular responses after implantation of bare BRS, sirolimus-eluting bioresorbable scaffold (SRL-BRS), and NVE-BRS. (A) Representative H&E-stained images and immunofluorescence images for CD31 and α-SMA in the bare BRS, SRL-BRS, and NVE-BRS groups. Asterisks indicate the scaffold struts. Scale bars, 50 μm. (B) Quantitative analysis of tunica intima thickness, CD31-positive deposition, and α-SMA-positive deposition in each group. Data are presented as mean ± SD. Statistical significance was determined using the two-sample t-test for tunica intima thickness and Mann-Whitney U test for CD31- and α-SMA-positive depositions. ***$p < 0.001$.

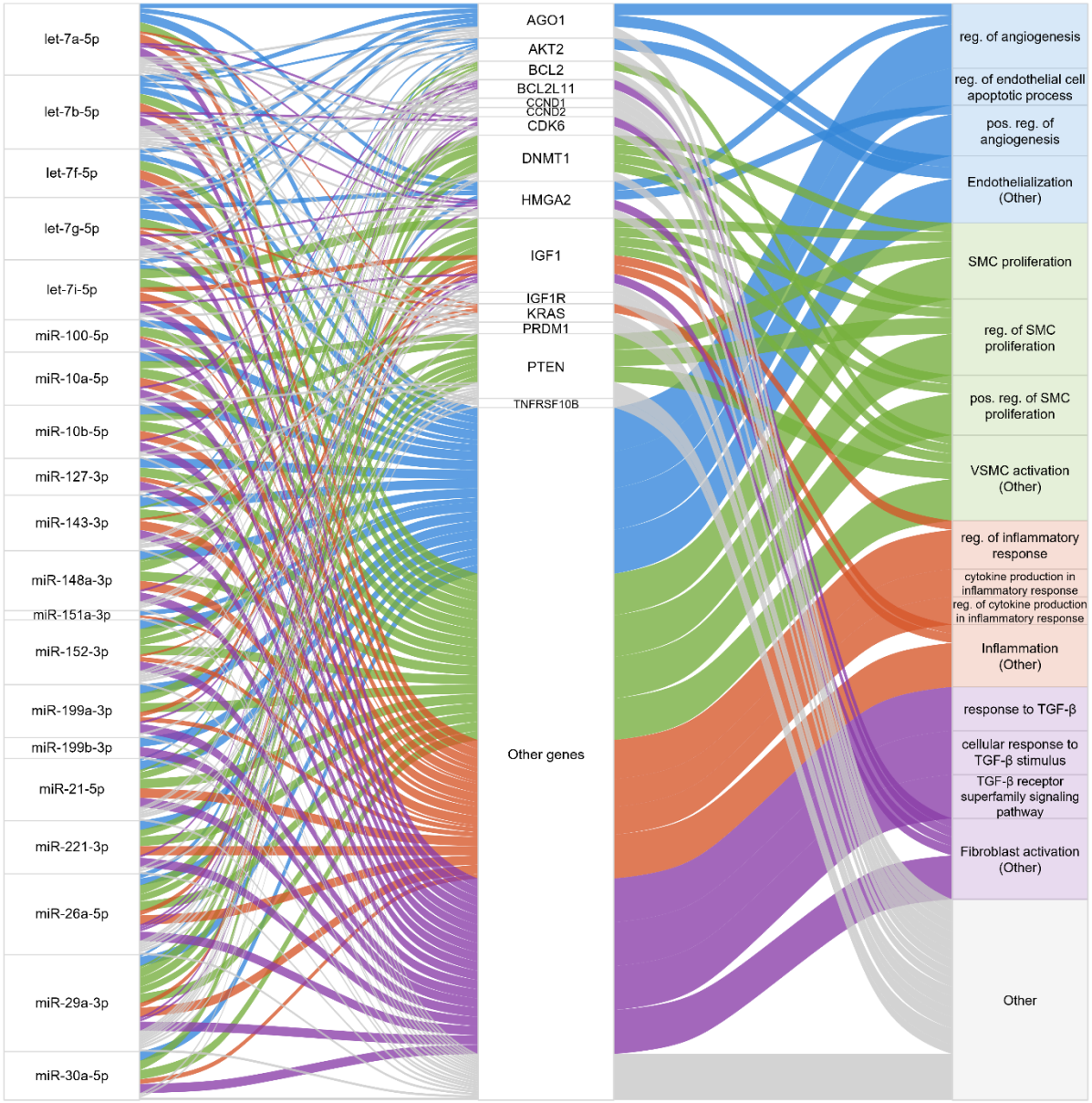


Figure S11. miRNA-target gene-GO term flow diagram for a representative subset of miRNAs (top 20 by normalized expression). Alluvial diagram connecting the top 20 miRNAs in MSC-NV (left) to their validated target genes (middle) and the GO Biological Process terms those genes are annotated to (right). Target genes shared by ≥4 of the top 20 miRNAs are shown individually; remaining genes are grouped as "Other genes." For each mechanism category, the 3 most significant GO terms are shown individually; remaining terms within that category are grouped as "{category} (Other)" and terms outside the four mechanism categories are grouped as "Other." Ribbon and label color indicate mechanism category (Endothelialization, blue; VSMC activation, green; Inflammation, orange; Fibroblast activation, purple; Other, grey).

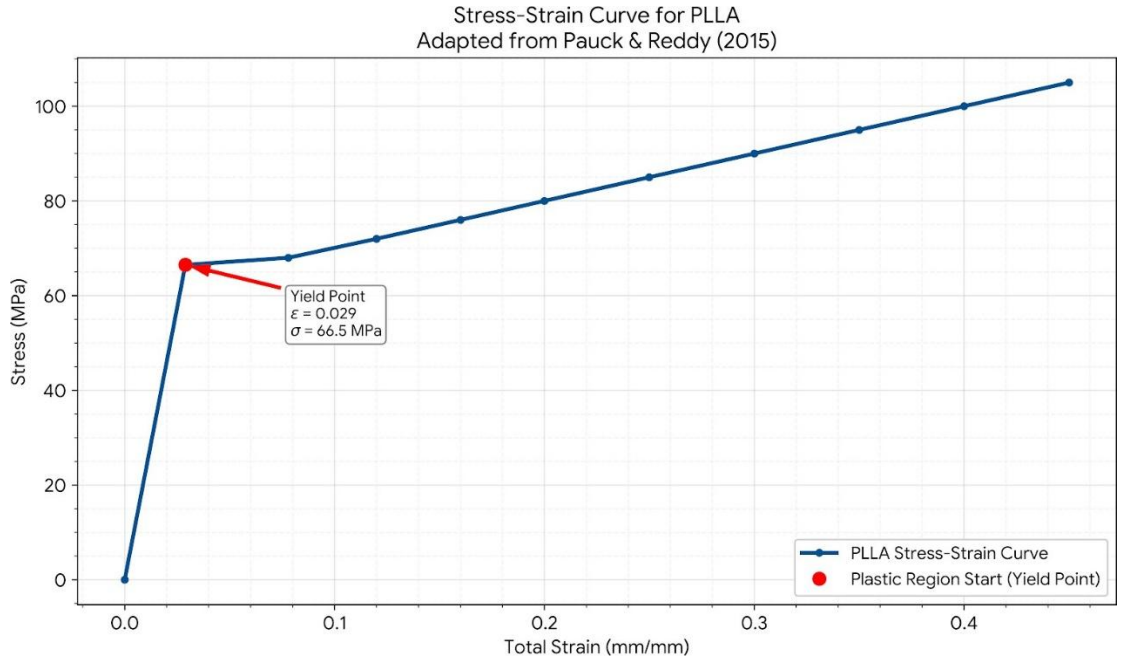


Figure S12. Total stress-strain curve for the PLLA stent material demonstrating multilinear isotropic hardening, adapted from Pauck and Reddy.[76]

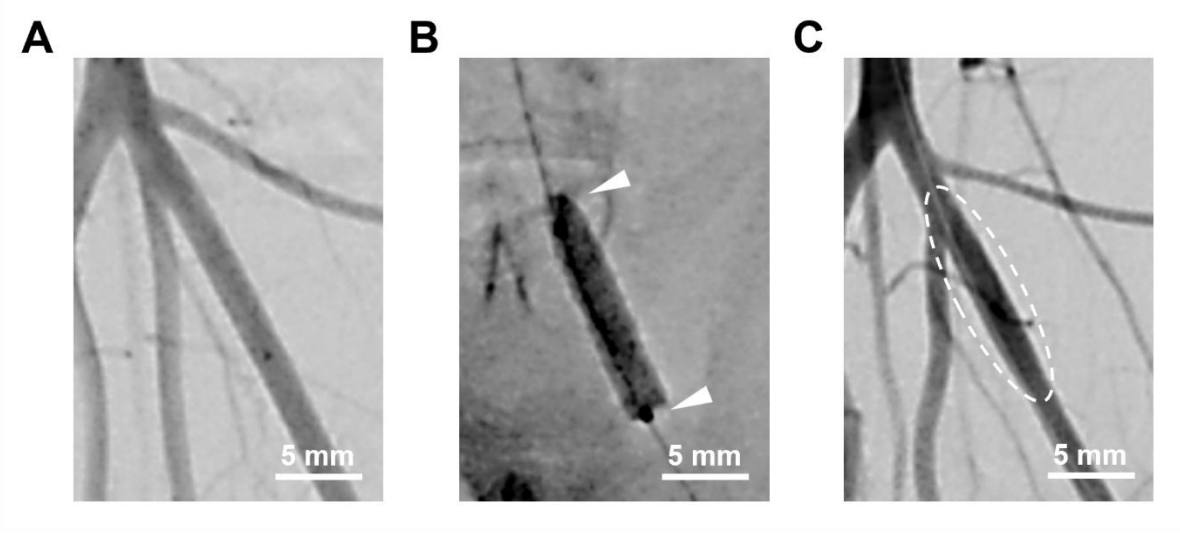


Figure S13. Technical steps for the creation of rabbit iliac arterial balloon-injury models. (A) Baseline angiographic image of the target iliac artery before balloon injury. (B) Balloon-induced arterial injury performed using a push-pull technique with repeated balloon dilation (white arrowheads, balloon markers). (C) Post-injury angiography demonstrating at the injured segment (white dashed circle).

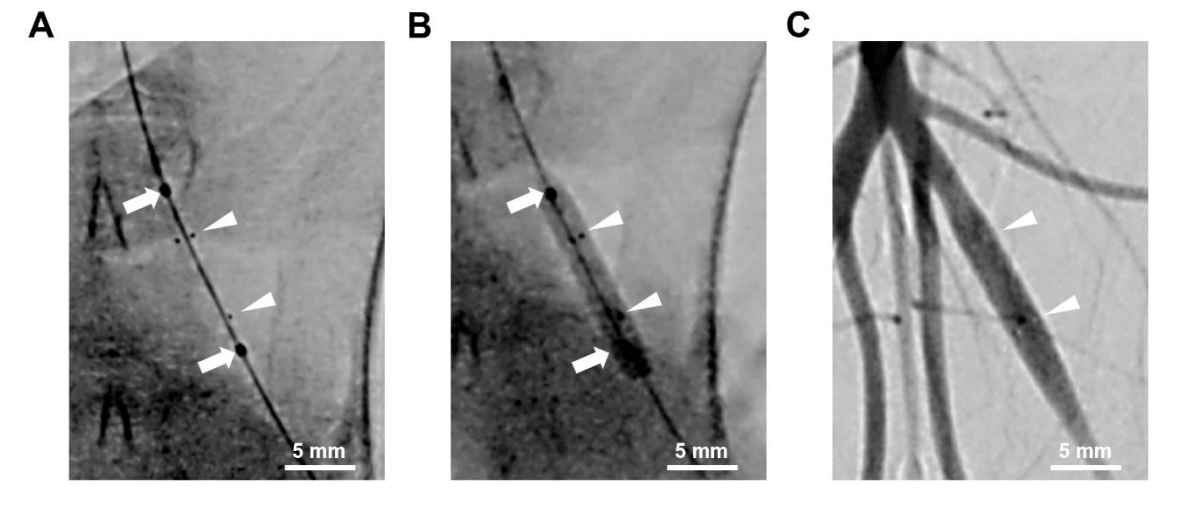


Figure S14. Representative angiographic images illustrating the step-by-step procedure for BRS implantation in the rabbit iliac artery. (A) Balloon catheter with mounted BRS positioned at the target lesion under fluoroscopic guidance (white arrows, balloon markers; white arrowheads, BRS radiopaque strut markers). (B) Balloon inflation to deploy the BRS at the injured iliac artery segment (white arrows, balloon markers; white arrowheads, BRS radiopaque strut markers). (C) Post-implantation angiographic image confirming appropriate BRS deployment and preserved luminal patency (white arrowheads, implanted BRS strut markers).